Research Article

Liling Zhang, Tiantian Zheng, Linliang Wu, Qi Han, Shiyu Chen, Yan Kong, Guicai Li*, Lei Ma, Hong Wu, Yahong Zhao, Yinxian Yu, and Yumin Yang*

Fabrication and characterization of 3D-printed gellan gum/starch composite scaffold for Schwann cells growth

https://doi.org/10.1515/ntrev-2021-0004 received November 27, 2020; accepted January 22, 2021

Abstract: Peripheral nerve injury has seriously affected patient's health and life. Schwann cells play an important role in peripheral nerve regeneration. However, the effect of the current tissue engineered scaffolds for promoting Schwann cells growth is still not as good as that of autologous graft. In this study, new developed three-dimensional gellan gum/starch (GG/ST) scaffolds with various printing gap for Schwann cells growth were prepared by 3D printing technology. Various physiochemical characterizations of the printed scaffolds were performed including morphology, rheological behavior, swelling ratio, and degradation behavior. The cytotoxicity and biocompatibility of the

scaffolds were evaluated using L929 fibroblasts and RSC96 Schwann cells, respectively. The results displayed that the GG/ST scaffold exhibited a porous network structure. The cross-sectional pore density of the hydrogel had a tendency to increase with the ascending printing gap. The swelling rate and degradation rate of the hydrogel gradually increased and eventually reached an equilibrium state. The rheological test results showed that the scaffolds had good printability. MTT cytotoxicity test and CCK-8 cell proliferation test displayed that the scaffold was nontoxic, and Schwann cells could grow well on the scaffold after 5 days of culture, whereas the number of cells on the scaffold with the printing gap of 3 mm was the largest. These results indicated that the GG/ST scaffold prepared by 3D printing technology may have a potential application in peripheral nerve regeneration.

Keywords: 3D printing, gellan gum, starch, peripheral nerve, scaffolds

Liling Zhang, Tiantian Zheng, Linliang Wu, Qi Han, Shiyu Chen, Hong Wu, Yahong Zhao: Key laboratory of Neuroregeneration of Jiangsu and Ministry of Education, Nantong University, 226001, Nantong, China; Co-innovation Center of Neuroregeneration, Nantong University, 226001, Nantong, China

Yan Kong: Key laboratory of Neuroregeneration of Jiangsu and Ministry of Education, Nantong University, 226001, Nantong, China Lei Ma: School of Information Science and Technology, Nantong University, Nantong, 226019, China

Yinxian Yu: Department of Orthopaedic Surgery, Shanghai General Hospital, Shanghai Jiao Tong University School of Medicine, Shanghai, 200080, China

1 Introduction

Peripheral nerve injury (PNI) is one of the global clinical diseases that seriously affects human health and life [1]. Autologous nerve transplantation is the golden standard for clinical repair of PNI, but the inadequate sources, mismatch of the size, and postoperative dysfunction limit its clinical application [2]. Currently, various natural biological materials, synthetic polymer materials, and composite materials have been widely used to fabricate scaffolds for PNI treatment [3]. But their effect on nerve regeneration is still not as good as autologous graft [4]. The reason may be ascribed to the unsuitable physicochemical properties of the scaffolds, such as porosity, pore size, etc., which may further influence adhesion and proliferation of cells [5]. Thus, tailoring the tissue engineering scaffold with appropriate geometries to enable nerve cells to better adhere and proliferate is of important

^{*} Corresponding author: Guicai Li, Key laboratory of Neuroregeneration of Jiangsu and Ministry of Education, Nantong University, 226001, Nantong, China; Co-innovation Center of Neuroregeneration, Nantong University, 226001, Nantong, China; Key Laboratory of Organ Regeneration & Transplantation of the Ministry of Education, Jilin University, 130061, Changchun, China, e-mail: gcli1981@ntu.edu.cn, tel: +86-0513-8505-1800

^{*} Corresponding author: Yumin Yang, Key laboratory of Neuroregeneration of Jiangsu and Ministry of Education, Nantong University, 226001, Nantong, China; Co-innovation Center of Neuroregeneration, Nantong University, 226001, Nantong, China, e-mail: yangym@ntu.edu.cn

significance for promoting nerve regeneration [6], which however has been seldom reported to date.

Generally, the tissue engineering scaffold prepared by traditional technology, such as freeze-drying and electrospinning, possesses various geometries with different porosity, pore size, mechanical properties, etc. However, it is difficult to obtain scaffolds with specially requested or uniform geometries due to the uncontrolled fabrication process. Three-dimensional (3D) printing technology can be used to prepare 3D biomaterials scaffolds with specific porosity and pore size for better simulating the microenvironment of cell ingrowth [7]. A composite hydrogel of alginate, fibrin, and hyaluronic acid/RGD peptide was prepared using 3D printing technology. Schwann cells were wrapped in the composite hydrogel to evaluate the effect of the scaffold on the cells. The results showed that the arrangement of cells in the scaffold could be wellregulated, indicating a huge application potential in the field of neural tissue engineering [8]. Ye et al. [9] used gelatin methacrylate (GelMA) hydrogel to print a multichannel hydrogel catheter with a length of 5 mm, and outer diameter of 6 mm, which was used to repair large gap nerve injury. The alginate hydrogels with low or high concentration of alginate were also used to prepare scaffolds with shells and cores structure through 3D printing technology. This unique combination method enables soft hydrogels to obtain 3D scaffolds with stable mechanical properties [10]. The interconnected pore structure in the 3D printing scaffolds could also provide sufficient space for cell connection, cell recognition and interaction, and nutrient transport [11]. Therefore, 3D printing technology can be used to well control the geometric structure of the scaffold for better cell growth and tissue regeneration.

Bio-ink is one of the key factors that affects the properties of the printed scaffolds. The biomaterials that are used as bio-ink should be biocompatible, nontoxic, and degradable [12]. For example, the enzyme-cross-linked silk fibroin (SF) was used as bio-ink to print a crescentshaped structural scaffold. The scaffold showed good mechanical properties and to be conducive to the adhesion of living cells. Moreover, the degradation of the scaffolds could be well-tailored for cell growth [13]. Besides, the SF/polyethylene glycol (PEG) was also developed as a bio-ink for printing a rectangular parallel-piped scaffold. Mixing PEG with SF could result in the formation of SF β-sheet structure, which could lead to gelation and water insolubility through physical cross-linking [14]. However, these materials usually need further cross-linking to maintain their structural integrity after printing. For example, cellulose has good biocompatibility and biodegradation while it is difficult to process, because cellulose is difficult to be dissolved in common solvents. For providing an efficient way to prepare natural cellulose hydrogel under room temperature, a kind of cellulose hydrogel scaffolds was firstly 3D-printed and then cross-linked using 0.8% N,N'-methylenebisacrylamide (MBA) solution. The mechanical properties were proven to be largely enhanced after cross-linking by MBA [15]. Nevertheless, for tissue engineering application, the cross-linking reagent may bring toxic substance to the scaffolds and be harmful for cell growth. Therefore, the development of new bio-ink with good mechanical properties and biocompatibility is necessary [16]. Gellan gum (GG) is an anionic polysaccharide produced by the Sphingomonas paucimobilis, which has been widely used in food as a gelling/stabilizing agent and also in bacterial culture systems [17,18]. Low concentrationed GG hydrogels using 3D extrusion techniques had been successfully developed for cartilage regeneration [19-21]. Nanomaterials with large specific surface area good characteristics of biocompatibility and biodegradability have achieved great success in the field of tissue engineering. Nanoparticles fabricated from nanomaterials or composed of general materials are commonly used as the reinforcement factors for various polymer matrix. Thus, nanocomposites have brought huge potential in the significant enhancement of performance for biomedical applications [22]. Starch is a polysaccharide composed of glucose units and exists in plant tissues in the form of amylose and amylopectin. The nano-sized starch has good fluidity when heated in an aqueous solution and can form firm gels when condensed [23,24]. Huang et al. used a gel-like corn starch network to improve the viscoelasticity and strength of the dough [25]. Mehboob et al. [26] fabricated starch with high elasticity and flexibility, which showed excellent mechanical properties and low water permeability. In addition, the biocomposites derived from a starch-glycerol biodegradable matrix reinforced with jute fibers aiming for replacing the expensive, hazardous, or depleting materials were fabricated by Verma et al. [27]. The addition of starch was shown to increase the viscosity of the biocomposites and endow a high swelling power and a low gelatinization temperature. Recently, a quickly formed 3D tissue structure-starch foam was prepared by Wen et al. [28], which proved that starch foam could encapsulate RSC96 cells and dorsal root ganglion (DRG), proving to be promising in nerve tissue engineering.

In this study, a GG/ST hydrogel scaffold was prepared using sol-gel technology and 3D printing technology. The hydrogel scaffold properties were evaluated by morphology, swelling test, degradation rate, and pore analysis. In addition, the toxicity of the scaffolds was tested using fibroblasts. The proliferation and cell growth morphology of the Schwann cell on the scaffold were evaluated to penetrate the potential application prospect of the scaffold in peripheral nerve regeneration. The study was anticipated to provide an experimental basis for the development of new artificial nerve grafts for neural tissue engineering. temperature is 17°C, the needle gauge is 19, and the thickness of the printing layer is 1 mm, The filling gap is 2, 2.5, and 3 mm, and the air pressure is 0.11-0.3 MPa. Then after 3D printing, the printed stent needs to be stored at -20°C for 48 h to fix its shape. Finally, before using the stent, freezedry the stent in a freeze dryer at -50°C for 36 h before use.

2 Materials and methods

2.1 Materials

The L929 fibroblast cell line was purchased from the ATCC cell bank in Shanghai, China, and the RSC96 rat Schwann cell line was purchased from the cell bank of the Chinese Academy of Sciences. GG was purchased from Yinuo Biotechnology Co., Ltd., China. Starch (ST) and paraformaldehyde (PA) come from National Pharmaceutical Group Chemical Reagent Co., Ltd., China. Tyr-Ile-Gly-Ser-Arg (YIGSR) peptides were bought from Shanghai Jier Biochemical Co., Ltd., China. Toluidine blue (TBO), Hoechst 33342, Cell Counting Kit-8 kit, penicillin-streptomycin (PS), and trypsin (Try) were all from Sigma-Aldrich, USA. MTT cell proliferation and toxicity kit and BCA protein concentration determination kit were from Biyuntian Co., Ltd., China. Fetal bovine serum (FBS) and DMEM high-sugar basal medium come from Gibco, USA. Phosphate buffer (PBS, pH7) was purchased from HyClone Co., Ltd.

2.2 Design and fabrication of GG/ST scaffolds

The model printed in this experiment is mainly a cuboid structure. Firstly, a model diagram of a cuboid structure was drawn in the software of solid works (2016 version), as shown in Figure 1. Then the model diagram was imported into the computer of the 3D printer for programming. Finally, the GG/ST scaffold was prepared by a 3D printer (Shining 3D, CN). The bio-ink was prepared as follows: 16 g GG powder with 4, 5.4, 8, and 16 g starch powder separately were dissolved in pure water at a temperature of 80°C thoroughly. After stirring and mixing evenly, the solution was left to cool at room temperature and then stored at 4°C overnight to obtain a printable bio-ink. Then, the mixed solution was transferred into the 3D printer, and GG/ST scaffolds were printed according to the designed model. First follow the steps to turn on the 3D printer, and set the 3D printer to print at a speed of 15–20 mm/s, the nozzle temperature is 40°C, the platform

2.3 Analysis and test

2.3.1 Atomic force microscope (AFM) and rheological evaluations

The size of starch was detected using AFM (FM-Nanoview6800). Briefly, the starch was blown to a clean coverslip surface to form a single layer, then a tap-mode of AFM was used to observe the morphology of starch particles. The size of starch particles was then statistically analyzed. The rheological properties of the hydrogel at room temperature were detected using the rheological test with a rotary rheometer (HAAKE RS6000, Thermo Fisher Science, USA). The GG/ST hydrogels for rheometer testing were prepared in advance according to the above method. The gap between torque and test platform was 1.2 mm, the mode was amplitude test, and the stress was determined to be 0.1%. Then, the prepared GG/ST hydrogel was added to the test platform with the dosage of 2 mL for measurement. The shear thinning characteristics of bio-ink were studied in dynamic mode, and the oscillatory strain sweep test was performed with 0.1% strain. The values of G' and G'' under the strain condition of 0.1% were obtained, and finally the loss factor is obtained.

2.3.2 Morphological observation

After 3D printing was completed, a digital camera (Huawei Nova2s, CN) was first used to observe the general appearance of the scaffolds. An optical microscope was then used to record the morphology of the scaffold, and the surface and cross-sectional micro-morphology of the hydrogel were analyzed by a scanning electron microscope (SEM). Secondly, the scaffold was frozen overnight at –20°C and then lyophilized in a freeze dryer (Shanghai De Xiang Co., Ltd.) for 48 h. The freeze-dried hydrogel samples were cut into two halves and divided into surface group and cross-section group. In order to observe the microstructure, two groups of scaffolds were fixed on the aluminum platform and coated with a layer of gold layer. The scaffolds were

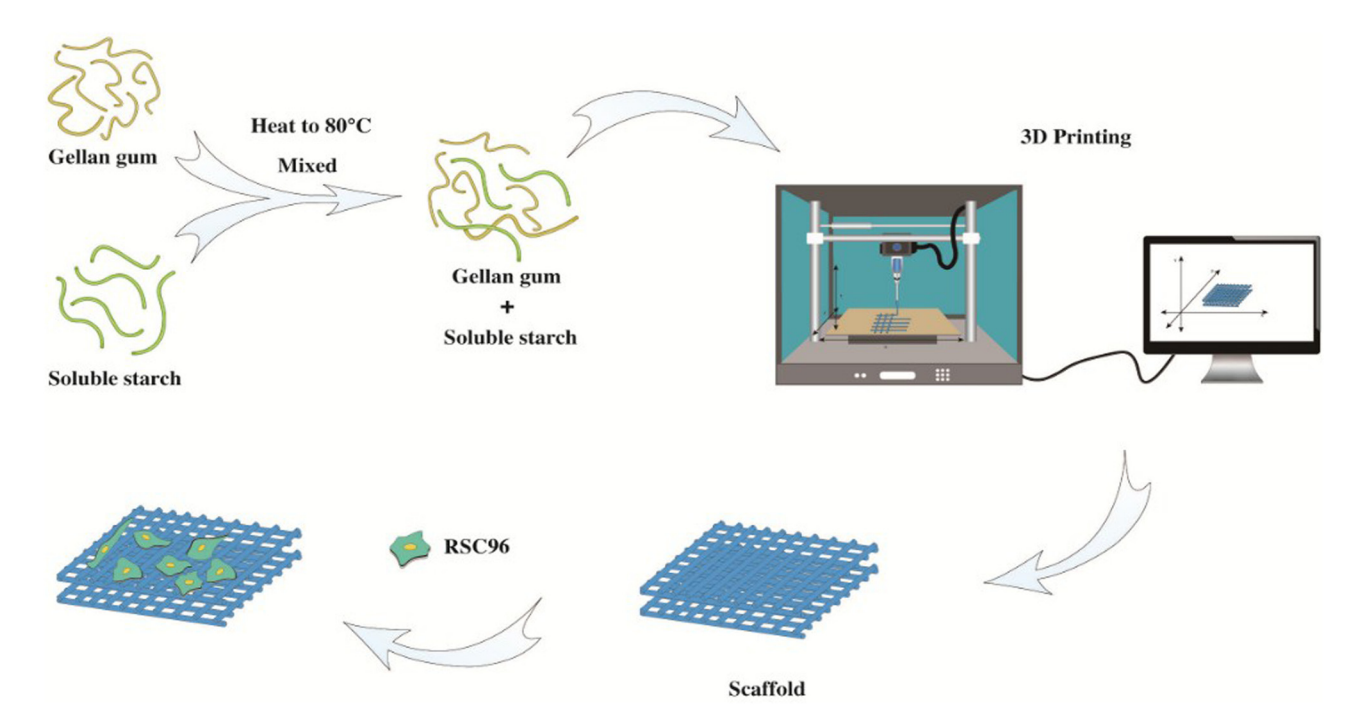


Figure 1: The preparation of the GG/ST hydrogel.

then observed using SEM, and the whole process was performed under vacuum condition of 1.4×10^{-4} bar.

2.3.3 Water uptake

Firstly, the scaffolds with the size of $0.5 \times 0.5 \times 3$ mm were freeze-dried and weighed; the initial mass was recorded as W_0 . Then the freeze-dried scaffolds were immersed in phosphate buffered saline (PBS, pH = 7.2). Finally, 10, 20, 30, 60, 90, 120 min and 3 days were chosen as the time interval for calculating the amount of water uptake. The sample was dried with filter paper at each time point and the mass was recorded as W_1 . Three parallel samples were tested for each sample. The swelling rate was calculated using the following formula:

$$S_{\rm R} = (W_1 - W_0)/W_0 \times 100\%$$

2.3.4 Porosity analysis

The porosity of the GG/ST scaffold is determined by the gas displacement method. In general, the lyophilized scaffolds with different printing gaps are immersed in a cylinder filled with absolute ethanol (V_1) for 10 min. Then, the total volume of the scaffold immersed in absolute ethanol was recorded as V_2 . Finally, the scaffold was taken out of the measuring cylinder, and the volume of

the remaining absolute ethanol was recorded as V_3 . Three parallel samples are tested for each scaffold. The calculation formula of porosity in this experiment is as follows:

Porosity (%) =
$$(V_1 - V_3)/(V_2 - V_3) \times 100\%$$

2.3.5 Degradation test

The initial mass of the lyophilized 3D scaffold with a size of $2 \times 2 \times 3$ mm was recorded as W_0 , and then the lyophilized scaffolds were immersed in PBS for 1, 2, 3, 5, 7, and 10 days, and the scaffolds were lyophilized again and weighed as $W_{\rm nd}$. Three parallel samples were tested for each sample. The degradation rate $W_{\rm d}$ of the scaffold *in vitro* was calculated by the following formula:

$$W_{\rm d}$$
 (%) = $(W_0 - W_{\rm nd})/W_0 \times 100\%$

2.4 Cell culture

2.4.1 Cytotoxicity

The three scaffolds were irradiated with ultraviolet light $(365 \, \text{nm}, \, 10 \, \text{mW/cm}^2, \, \text{ENF-260C/FA}, \, \text{Spectroline}, \, \text{USA})$ for 30 min, and then soaked in 75% ethanol for 30 min and washed with PBS (pH = 7.2) 3 times, each time for 10 min. The scaffold was immersed in 10 mL DMEM

medium and incubated for 24 h. Then, the medium was collected in a 50 mL centrifuge tube and used for L929 culture. The cells density was 5×10^3 cells/mL. After 24 h and 48 h of culture, 10 μL of MTT reagent was added to each well and incubated. After further culture for 4 h, the reagent was removed and 100 μL of formazan lysis buffer was added. After another 4 h, the supernatant with 150 μL from each sample was transferred to the 96-well plate in a microplate reader for absorbance detection at a wavelength of 570 nm.

2.4.2 CCK-8 test

The scaffold material was sterilized by ultraviolet light for 30 min and immersed in 75% ethanol for 20 min, and then washed with PBS three times, each time for 10 min. Then $10\,\mu\text{L}$ of cell suspension with a density of 5×10^4 cells/mL was added to the scaffolds and incubated at 37°C in a CO₂ incubator for 1, 2, and 3 days, respectively. After that, the culture medium was discarded, and $500\,\mu\text{L}$ of CCK-8 solution was added to each well and incubated in an incubator for 4 h. Then, $200\,\mu\text{L}$ of the solution was taken from each well and added to a 96-well plate, eight parallel samples were used, and the OD was measured at 450 nm.

2.4.3 Schwann cells culture

The RSC96 Schwann cells were used for evaluating the biocompatibility of the printed scaffolds. Before cell culture, the scaffolds were pretreated using YIGSR polypeptide (50 $\mu g/mL$) for 2 h for enhancing cell adhesion. Then, RSC96 cells were seeded on GG/ST scaffold at a cell density of 1×10^5 cells/mL and incubated for 1, 3, and 5 days, respectively. At each time point, cells were fixed with 4% PA for more than 4 h and washed 3 times with physiological saline. Thereafter, 50 μL of hoechst33342 diluted 1:20 in PBS was added to the cells and kept in the dark for 30 min. Finally, the scaffolds were washed with physiological saline for five times. The cell growth status was observed under an inverted fluorescence microscope (Leica, Germany).

2.5 Statistics

All the experimental results were analyzed by Origin 8.0 (Origin Lab company) and Image Tool. The results were

expressed as mean \pm standard deviation (SD). p values of < 0.05 (p < 0.05) were considered as significant.

3 Results

3.1 AFM and rheological characteristics

Figure 2(a and b) shows the morphology of starch by AFM. The starch particles were arbitrarily deposited on the glass slide (Figure (2a)). Through statistical analysis of the image, the size of the starch nanoparticles was approximately 140 nm (Figure (2b)). Figure 2(c and d) is the rheological characteristics of GG/ST hydrogel. The storage modulus (G') of the four ratios of GG/ST scaffolds were all greater than the loss modulus (G''), which proved that the hydrogel was formed. In Figure (2b), The Loss factor, namely loss angle (tan θ), is the ratio of loss modulus (G'') to storage modulus (G'), which mainly reflects the viscoelastic ratio of the material. The greater the loss factor, the greater the viscosity of the material, and the smaller the loss factor, the greater the elasticity of the material. When $\tan \theta > 1$, G'' > G', the hydrogel behaves as a sol, while when $\tan \theta < 1$, G'' < G', the hydrogel behaves in a gel state [29]. During the experiment, the concentration of GG was kept at 16%, and starch was added in the ratio of 1:4, 1:3, 1:2, 1:1. The increase in starch concentration had a great effect on the viscoelasticity of the system. When the ratio of ST and GG was 1:1 and 1:2, the elasticity of the material was high, which was not conducive to material extrusion. When the ratio is 1:4, the viscosity was too large and the material was too easy to extrude, which was not conducive to maintain the scaffold structure; therefore, the concentration ratio of all samples in the later period remained 1:3. These results indicated that the GG/ST scaffolds had the capability for 3D printing.

3.2 Morphology of the scaffolds

The surface and cross-section of the 3D-printed scaffolds at different gap were observed by SEM (Figure 3(a1–a4)). With the increased printing gap, the pore size on the hydrogel surface increased first and then decreased. The possible reason is that when the length and width of the printing model are determined, with the increase of the printing gap, the number of turns that the printing needle needs to rotate decreases, and the extrusion force

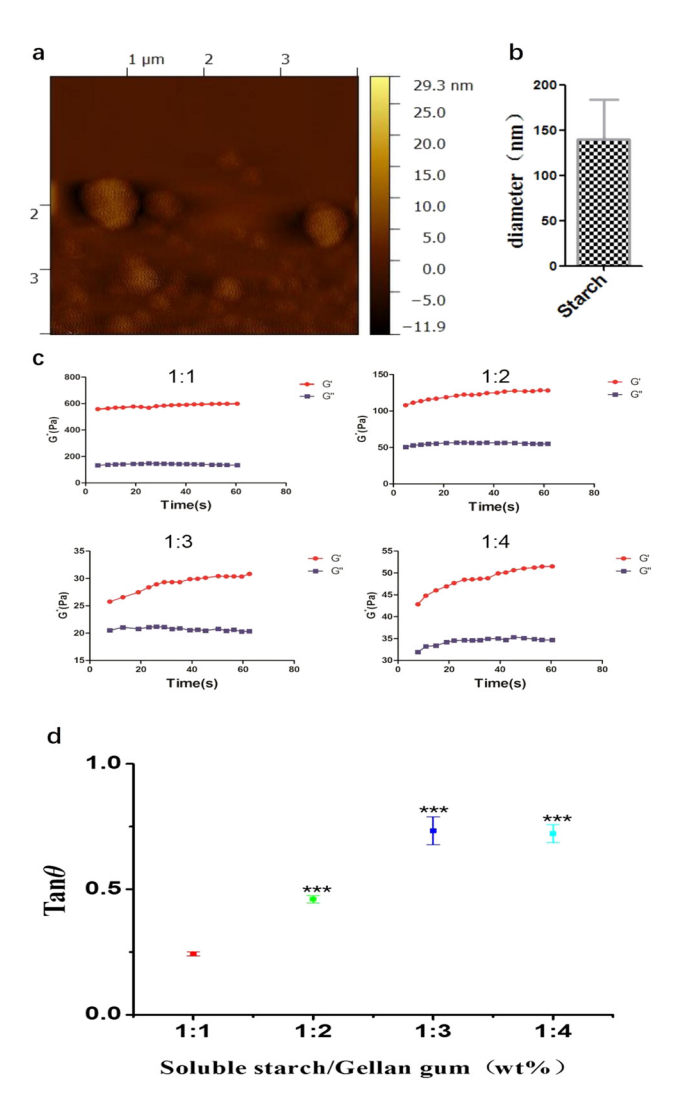


Figure 2: AFM of starch granules and rheological properties of GG/ST scaffolds with different ratios. (a) AFM; (b) starch particle size; (c) G' and G'' in amplitude mode; (d) loss angle. ***p < 0.001 by one-way ANOVA test.

will change to a certain extent, so the aperture becomes larger. At the same time, when the printing distance is greater than 2.5 mm, the internal extrusion force can change in enough time, resulting in the aperture size less than 2.5 mm. Quantitative analysis was shown in Figure 3(b); when the gap was 2.5 mm, the surface and internal pore sizes of the hydrogel were larger than other hydrogels regardless of the surface or cross-section. As shown in Figure 3(c), when the scaffold printing gap was 2 mm, the number of pore density reached a maximum of 1,220 pores/mm², and when the gap was 2.5 mm, the number of pores reached a minimum of about 360 pores/mm². In Figure 3(d), when the printing gap was 2 mm and 2.5 mm, the porosity was around 90%,

and when the printing gap further increased to 3 mm, the porosity dropped to 45%.

3.3 Swelling behavior

Figure 4 shows the swelling behavior of 3D-printed scaffolds with different printing gaps in deionized water. Each scaffold gradually reached equilibrium swelling from 0 to 3 days. When the scaffolds' printing gap was 2 mm, the swelling ratio was between 380 and 440%. which was lower than that of other groups. When the printing gap of the scaffold was 2.5 mm, the swelling rate increased steadily before 1h, and there was a tendency for the swelling rate to decrease after 1 h. For this phenomenon, the solvent first infiltrated the surface of the scaffold, and then slowly dipped into the interior until equilibrium was reached. Since the pore size on the surface of the 2.5 mm scaffold was smaller than the inner pore size, the swelling rate increased after 1 h and then gradually stabilized. When the printing gap of the scaffold was 3 mm, the increased rate of the swelling rate was less than 2.5 mm before 1 h, but higher than 2.5 mm after 1h. The reason why the swelling rate of the 3 mm group was higher than 2.5 mm group at the last time may be that the cross-section and the number of pores on the surface of the 2.5 mm group are smaller than those of the 3 mm group.

3.4 Degradation behavior

The degradation behavior of the prepared three scaffolds in PBS was studied, and the mass loss from 0 to 10 days was recorded. As shown in Figure 5, when the printing gap of the scaffolds was between 2.5 and 3 mm, the degradation rate of the scaffolds increased steadily from day 1 to day 2, indicating that the formation of hydrogel did not reduce its own water absorption performance. The degradation rate of the scaffolds dropped sharply from 2 to 3 days and showed an upward trend from 3 to 4 days, and eventually gradually stabilized. The degradation rate required multiple freeze-drying and soaking in PBS. It was noticed that the degradation rate on the third day decreased, which may be caused by the solvent that was not being completely lyophilized. The scaffolds with a spacing of 2 mm always maintained a stable degradation rate, which also was in accordance with the results of swelling rate. In contrast, the degradation rates of 2.5 mm

Figure 3: Morphological characterization of GG/ST scaffold. (a) Cross-sectional view of the scaffolds taken by scanning electron microscope; (b) quantitative analysis of the cross-sectional pore density; (d) porosity test. *p < 0.05 by one-way ANOVA test.

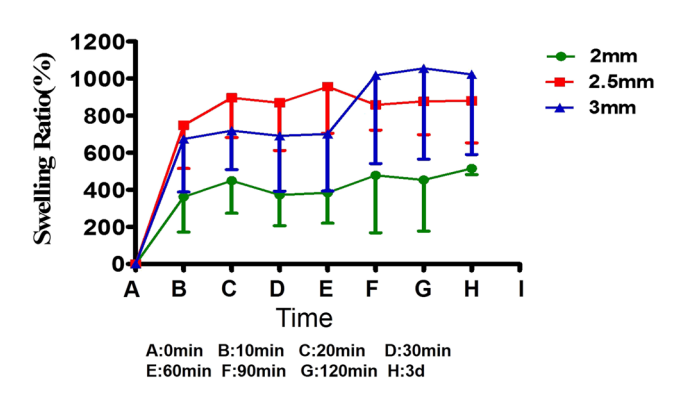


Figure 4: Swelling ratio test of GG/ST scaffold with various printing gap. *p < 0.05 by one-way ANOVA test.

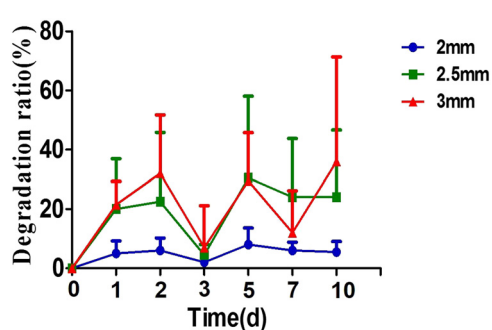


Figure 5: Degradation experiment of GG/ST scaffold.

scaffolds and 3 mm scaffolds varied heavily. This result indicated that the degradation rate of printed scaffolds with various printing gap was different.

3.5 Cytotoxicity

Figure 6(a) shows the results of L929 fibroblast on printed scaffolds with different gaps after 3 days of culture. Cells were distributed on the surface of all scaffolds. However, the cells still showed certain aggregation. After 3 days, all the cells on the scaffold were obviously spread out. Overall, the cells on the 2 mm scaffold were less than those on 2.5 and 3 mm groups. The cells on the 2.5 and 3 mm groups covered almost the entire surface of all

scaffold. The results showed that the prepared composite hydrogel was suitable for cell adhesion and proliferation without obvious cytotoxicity. Figure 6(b) shows that the absorbance of the three scaffolds was significantly higher than that of the control group, which proved that the scaffolds were basically nontoxic. The CCK-8 results in Figure 6(c) show that the absorbance of the three scaffolds increased steadily from 1 day to 3 days, which indicated that the cell viability of the cells on the scaffold was continuously rising and could grow well on the scaffold. After 3 days of cell culture, the cell viability on the scaffold with 2.5 mm gap was higher than that in the control group. This may be because the pore size of the scaffold in the 2.5 mm size was larger on the surface and inside than the other groups, which was good for nutrients to penetrate into the scaffold and cells growth.

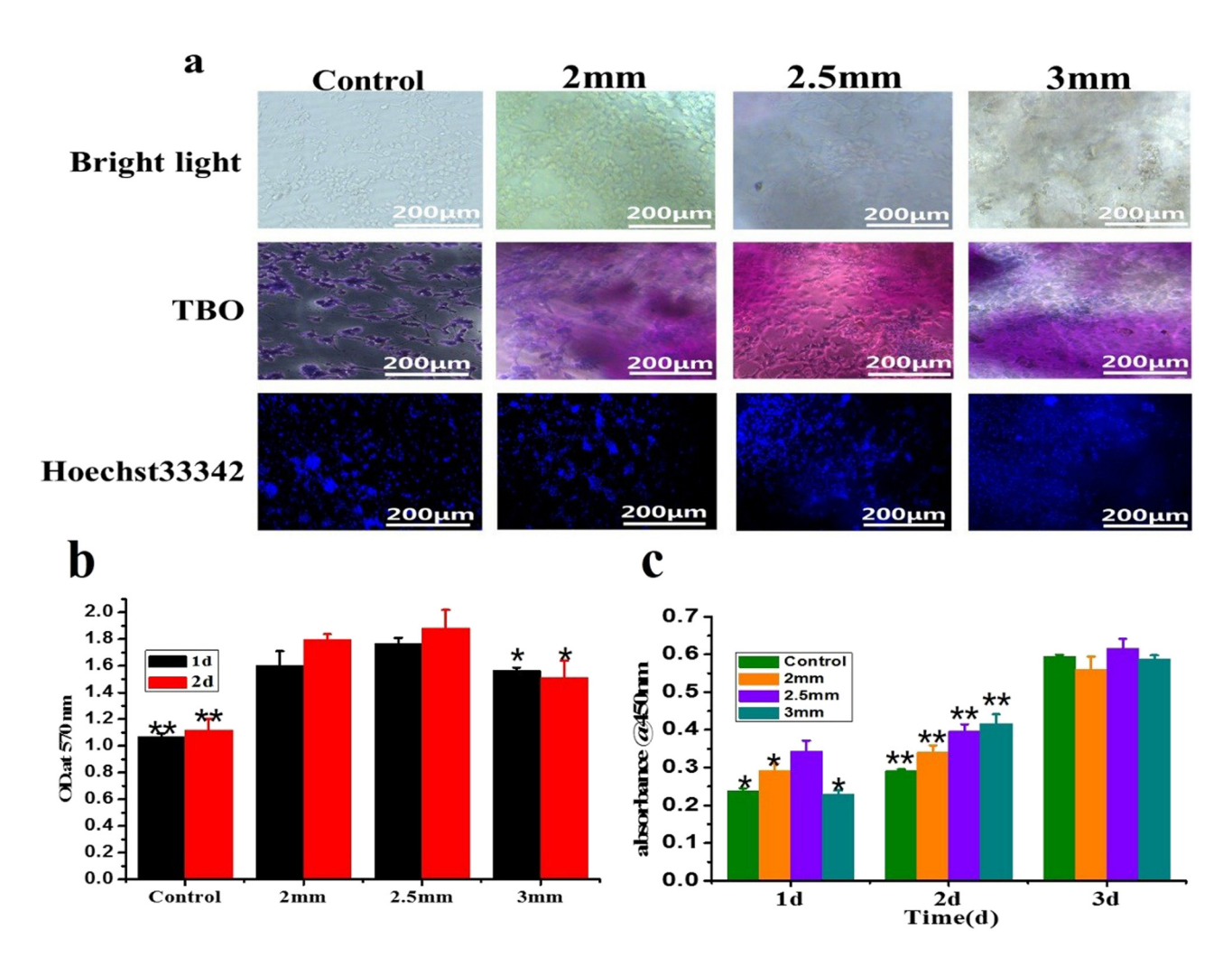


Figure 6: Cell morphology and toxicity of GG/ST scaffolds. (a) TBO and immunofluorescence; (b) MTT test cytotoxicity experiment; (c) cell viability detection. *p < 0.05 and **p < 0.01 by one-way ANOVA test.

58 — Liling Zhang et al. DE GRUYTER

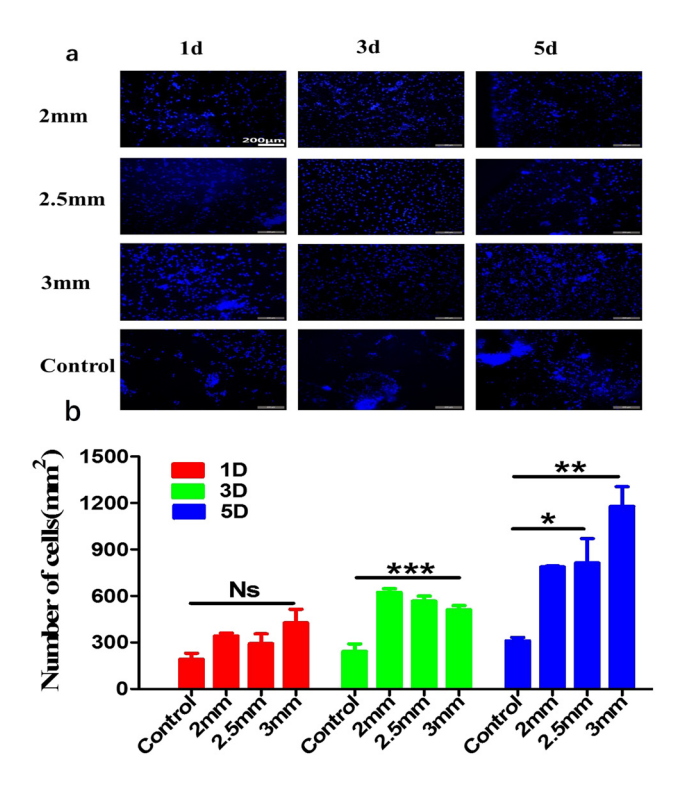


Figure 7: Schwann cells culture. (a) Immunofluorescence images of GG/ST scaffold cocultured with RSC96 cells for 1d, 3d, and 5d. (b) Statistics of cell count results related to immunofluorescence. *p < 0.05, **p < 0.01 and ***p < 0.001 by one-way ANOVA test.

3.6 Schwann cells evaluation

RSC96 cells were cultured in GG/ST scaffold for 1, 3, and 5 days to evaluate the effect of the scaffold on nerve regeneration. As shown in Figure 7(a), the number of cells in the scaffold group was significantly more than that in the control group. Moreover, cells in control group displayed obvious aggregation than the scaffolds group. The quantitative analysis of immunofluorescence is shown in Figure 7(b). The results show that the number of cells in the experimental group was higher than that in the control group. After 5 days of cultivation, the number of cells in the 3 mm group was significantly higher than that in the other groups, while the number of cells in the 2 and 2.5 mm groups was basically the same.

4 Discussion

Currently, the clinical application of autologous nerve transplantation is still the gold standard for peripheral nerve regeneration [30]. However, due to the limited

sources of autologous transplantation and the loss of donor site function, autologous nerve transplantation is usually a clinically conservative treatment [31]. Thus, the artificial nerve grafts that replace autotransplantation have been developed. 3D printing technology could construct nerve implants with excellent performance for nerve regeneration; however, the bio-ink for 3D printing still needs to be further improved. In this study, a new type of bio-ink composed of GG and nano-sized starch was developed. GG/ST scaffolds with different printing gaps were prepared by 3D printing technology. The GG/ST scaffold was basically noncytotoxic and the cells proliferated stably. When the printing distance was 3 mm, the growth state and morphology of Schwann cells in the scaffold were the best, showing high cell survival rate and the largest number of cells. Therefore, the GG/ST scaffold prepared by 3D printing technology may have potential applications in peripheral nerve regeneration and provide an important experimental basis for the development of peripheral nerve grafts.

The maximum concentration of GG for preparing the GG/ST composite scaffolds was determined to be 16 wt%. At a shear rate of 100 s⁻¹, except for the ratio of GG and starch of 1:1, which did not show shear thinning behavior, the other ratios of 1:2, 1:3, and 1:4 all showed this behavior. As described by Malda et al. [32], the shear thinning was very important for extrusion-based printers. Although the three ratios all exhibited shear thinning behavior, the ink with ration of 1:2 could not be printed depending on the pressure of the 3D printer itself. When the ratio was 1:4, the material was particularly easy to extrude, but it was not easy to maintain the structural integrity, while easy to collapse. Thus, a ratio of 1:3 was chosen for the sequential experiment.

The composite material of GG and starch had a highly interconnected pore network and a high total internal porosity. All printed scaffolds had a porous structure, which was an important indicator of nutrient exchange in tissues [33]. In our study, as shown in Figure 3(d), all scaffolds except the 3 mm scaffold exhibited porosity higher than 90%, which was of great benefit for material exchange and nutrient transport. The reason may be that the density of the surface holes of the 2 mm group was greater than that of the 3 mm group, and the number of surface holes was more than that of the 3 mm group. Compared with the scaffolds of the 2.5 mm group, the size of the surface and the inner hole was larger than that of the scaffold of the 3 mm group. The hole diameter of the 2 mm and 3 mm scaffolds was smaller than that of the 2.5 mm scaffold. The possible reason was that the printing gap of 2.5 mm was the best setting data for the 3D printer, and the dual network structure of GG/ST was obtained. Significant differences in the number of pores formed and pore size distribution were also observed (Figure 3). It may be speculated that the freeze-dried double-network hydrogel was responsible for these inherent differences. Previous studies reported that in composite scaffolds, the formation of a network structure kept the structure more stable, thereby making the structure more resistant to shrinkage and expansion [34].

The swelling ability of the hydrogel was further evaluated. This experiment was achieved by soaking the hydrogel in deionized water. Proper swelling of the hydrogel will help to expand the spacing between the various molecules in the hydrogel and facilitate cell ingrowth and nutrient exchange between cells [35]. The printed scaffold structure is easy to diffuse between ions and leads to a soft structure, which increases the absorption of water. The pore density has a certain relationship with the swelling rate of the scaffold [36,37]. The larger the pore density, the higher the swelling rate. It is obvious from Figure 4 that the swelling rate of 2 mm had always been lower than that of 2.5 and 3 mm scaffolds, but the swelling rate of 2.5 mm was initially higher than 3 mm, and the final expansion rate is lower than 3 mm. This result was the same as that of the 3 mm group with a higher pore density than the other two groups. The stability of the hydrogel could provide a stable platform and microenvironment for cell growth and tissue regeneration [9]. Three groups of scaffolds were immersed in PBS to evaluate the degradation behavior. The 2 mm scaffolds structure had always maintained a stable degradation rate of around 5%, while the degradation rates of the 2.5 and 3 mm scaffolds were basically maintained at 35%, which was consistent to the porosity results. Compared with the 2 mm scaffold, the scaffold of 2.5 and 3 mm had larger surface and internal holes, and the density of the internal pores of the scaffold was also larger. This facilitated the separation of solvents into the scaffold and the solvent molecules gradually diffused into the scaffold. Inside the scaffold, the volume of the polymer material was continuously increasing, and the movement of the macromolecular segment was enhanced, and then the movement of the entire macromolecular chain was achieved through the coordinated movement of the segment, and the macromolecule gradually entered the solution to form a thermodynamically stable homogeneous system, thus the scaffold with different print gaps showed different degradation ratio. Our results indicated that these three scaffolds possessed a certain degradation rate, while the degradability of the scaffold provided a possibility for future clinical application [38,39]. Finally, the cytotoxicity and effect on

nerve cells of the printed GG/ST scaffolds were evaluated. Though GG had been applied for skin tissue regeneration in the previous study and cell could proliferate well without cytotoxicity [40], no studies referring to the effect of GG on nerve cells was reported. Thus, considering the effect of the scaffolds on cell viability, L929 fibroblast culture was first used to evaluate the cytotoxicity of the prepared scaffolds. With the extension of the culture time, the cells proliferated significantly, indicating that all scaffolds had no significant toxic effects on the cells. The CCK-8 experiment results also confirmed the finding, which was in accordance with the previous study. There are two possible reasons for this. One is that the selected material, GG, is a food-grade material, an extracellular heteropolysaccharide gum produced by aerobic fermentation of Sphingolipids under neutral conditions. In addition to increasing its mechanical strength, starch itself is also a polysaccharide polymerized by glucose. On the other hand, since GG/ST mixes to form a loose and porous hydrogel, it facilitates nutrient exchange and waste discharge between cells and promotes cell growth. Schwann cells are glial cells that play a major supporting role in peripheral nerve regeneration [41]. Thus, RSC96 Schwann cell was cultured on the scaffold to evaluate the effect on peripheral nerve regeneration. As shown in Figure 7(a), the cells in the experimental group did not have obvious aggregation when they grew, but the control group could find obvious aggregation of the cells. Moreover, the number of cells in the experimental group was significantly more than that in the control group. As shown in Figure 7(b), RSC96 cells and scaffolds were cultured for 1, 3, and 5 days later; the number of cells in the experimental group was higher than that in the control group. The possible reason is that the printing gap of the 3 mm group scaffold is larger, the cross-sectional hole density is higher than the other 2 groups, and the internal pore size is larger and connected, which is conducive to material exchange and nutrient transportation. Generally, cells will have a higher survival rate in a porous network with cell binding domains on the scaffold [42]. Lozano et al. [43] also observed that the large pore density of the scaffold surface and cross-section could form a porous network structure, which was more conducive to the exchange of nutrients. The cell survival rate and cell viability were better. After 5 days of cell culture, the swelling rate of the 3 mm group was the highest among the three groups of scaffolds and reached a balanced state. The swelling rate of hydrogel is conducive to the exchange of nutrients in cells [44]. As Akkineni et al. [45] reported, the swelling rate of the scaffold was of great significance for in vitro cell culture experiments and implantation. The

16.7% sodium alginate and 3% GG scaffolds have the highest expansion rate in PBS, and human bone marrow mesenchymal stem cells (HMSC) have the highest cell number after 7 days of culture on the scaffold. As the printing gap increases, the degradation rate of the scaffolds increases and the degradation time shortens. The 2 mm group scaffold has always maintained a low degradation rate, which was not conducive to peripheral nerve regeneration. Although the degradation rate of the 2.5 mm group has increased, the degradation rate may be not still insufficient, which needs further investigation. Shi et al. [46] reported that the SF/gelatin scaffold with a degradation rate of about 37% was better for cell growth and spreading. In this experiment, the degradation rate of the 3 mm scaffold group was about 37%, and the number of cells was higher than that of other groups. Peng et al. [47] and other experiments also proved that the degradation rate can regulate the cell behavior of stem cells. It is reasonable to speculate that the degradation rate may have a certain influence on cell behavior.

5 Conclusion

In this study, GG/ST scaffolds with different printing gaps were prepared by sol-gel technology and 3D printing technology. The scaffolds with cuboid structure possessed suitable physiochemical properties, including porosity, swelling, degradation, etc., which may be better for tissue engineering implantation. Both L929 fibroblasts and RSC96 Schwann cells showed that the scaffolds had good biocompatibility without cytotoxicity. Moreover, the proliferation and cell growth morphology of Schwann cells on the scaffold with larger printing gaps were better than that with smaller printing gap. In summary, the GG/ST scaffold developed by 3D printing technology may have potential applications in peripheral nerve regeneration. The study may provide an important experimental basis for the design and development of artificial implants for treating peripheral injuries.

Acknowledgments: The authors gratefully acknowledge the assistance from Yi Zhu.

Funding information: The authors gratefully acknowledge the financial support of the National Natural Science Foundation of China (31830028, 31771054), Natural Key Science Research Program of Jiangsu Education Department (19KJA320006), the Open Project of Key Laboratory of Organ Regeneration and Transplantation,

Ministry of Education (2020JC08), Qinglan Project of Jiangsu Province (2018).

Author contributions: All authors have accepted responsibility for the entire content of this manuscript and approved its submission.

Conflict of interest: The authors state no conflict of interest.

References

- Grinsell D, Keating CP. Peripheral nerve reconstruction after [1] injury: a review of clinical and experimental therapies. Biomed Res Int. 2014;2014:698256.
- Ebrahimi MH, Samadian H, Davani ST, Kolarijani NR, Mogharabian N, Salami MS, et al. Peripheral nerve regeneration in rats by chitosan/alginate hydrogel composited with Berberine and Naringin nanoparticles: in vitro and in vivo study. J Mol Liq. 2020;318:114226.
- Matyga AW, Veen SC, Gasiorowski JZ. Natural and synthetic extracellular matrix biomaterials for peripheral nerve regeneration. In Vitro Cell Dev Biol Animal. 2018;54:27-32.
- Jia C, Luo BW, Wang HY, Bian YQ, Li XY, Li SH, et al. Precise and arbitrary deposition of biomolecules onto biomimetic fibrous matrices for spatially controlled cell distribution and functions. Adv Mater. 2017;29(35):282-6.
- Cai SX, Wu CX, Yang WG, Liang WF, Yu HB, Liu LQ. Recent advance in surface modification for regulating cell adhesion and behaviors. Nanotechnol Rev. 2020;9(1):971-89.
- Wu J, Xie LL, Lin WZY, Chen QS. Biomimetic nanofibrous scaffolds for neural tissue engineering and drug development. Drug Discov Today. 2017;22(9):1375-84.
- [7] Hofmann M. 3D Printing gets a boost and opportunities with polymer materials. Acs Macro Lett. 2014;3(4):382-6.
- Ning LQ, Sun HY, Lelong T, Guilloteau R, Zhu N, Schreyer DJ, et al. 3D bioprinting of scaffolds with living Schwann cells for potential nerve tissue engineering applications. Biofabrication. 2018;10(3):234-45.
- [9] Ye W, Li H, Yu K, Xie C, Wang P, Zheng Y, et al. 3D printing of gelatin methacrylate-based nerve guidance conduits with multiple channels. Mater Des. 2020;192:108757.
- [10] Akkineni AR, Ahlfeld T, Lode A, Gelinsky M. A versatile method for combining different biopolymers in a core/shell fashion by 3D plotting to achieve mechanically robust constructs. Biofabrication. 2016;8:4.
- [11] Ma HS, Luo J, Sun Z, Xia LG, Shi MC, Liu MY, et al. 3D printing of biomaterials with mussel-inspired nanostructures for tumor therapy and tissue regeneration. Biomaterials. 2016:111:138-48.
- [12] Donderwinkel I, van Hest JCM, Cameron NR. Bio-inks for 3D bioprinting: recent advances and future prospects. Polym Chem UK. 2017;8(31):4451-71.
- [13] Lode A, Meissner K, Luo YX, Sonntag F, Glorius S, Nies B, et al. Fabrication of porous scaffolds by three-dimensional plotting of a pasty calcium phosphate bone cement under mild conditions. J Tissue Eng Regen Med. 2014;8(9):682-93.

- [14] Zheng ZZ, Wu JB, Liu M, Wang H, Li CM, Rodriguez MJ, et al. 3D Bioprinting of self-standing silk-based bio-ink. Adv Healthc Mater. 2018;7:6.
- [15] Hu XZ, Yang ZJ, Kang SX, Jiang M, Zhou ZW, Gou JH, et al. Cellulose hydrogel skeleton by extrusion 3D printing of solution. Nanotechnol Rev. 2020;9(1):345-53.
- [16] Ferris CJ, Gilmore KG, Wallace GG, Panhuis MIH. Biofabrication: an overview of the approaches used for printing of living cells. Appl Microbiol Biot. 2013;97(10):4243-58.
- [17] Fan YT, Yi J, Hua X, Zhang YZ, Yang RJ. Preparation and characterization of gellan gum microspheres containing a coldadapted beta-galactosidase from Rahnella sp R3. Carbohyd Polvm. 2017:162:10-5.
- [18] Oliveira IM, Goncalves C, Shin ME, Lee S, Reis RL, Khang G, et al. Anti-inflammatory properties of injectable betamethasone-loaded tyramine-modified gellan gum/silk fibroin hydrogels. Biomolecules. 2020;10:10.
- [19] Silva-Correia J, Oliveira JM, Caridade SG, Oliveira JT, Sousa RA, Mano JF, et al. Gellan gum-based hydrogels for intervertebral disc tissue-engineering applications. J Tissue Eng Regen Med. 2011;5(6):97-107.
- [20] Melchels FPW, Dhert WJA, Hutmacher DW, Malda J. Development and characterisation of a new bioink for additive tissue manufacturing. J Mater Chem B. 2014;2(16):2282-9.
- [21] Kesti M, Muller M, Becher J, Schnabelrauch M, D'Este M, Eglin D, et al. A versatile bioink for three-dimensional printing of cellular scaffolds based on thermally and photo-triggered tandem gelation. Acta Biomater. 2015;11:162-72.
- [22] Jian W, Hui D, Lau D. Nanoengineering in biomedicine: current development and future perspectives. Nanotechnol Rev. 2020;9(1):700-15.
- [23] Wang GX, Li S, Feng YL, Hu YX, Zhao GY, Jiang W. Effectively toughening polypropylene with in situ formation of core-shell starch-based particles. Carbohyd Polym. 2020;249:116795.
- [24] Shan JQ, Liu DG, Su F, Li MY, Tian HF, Guo MN, et al. Anisotropic structure and properties of chitin and chitosan nanofibril-supported starch foams. ACS Sustain Chem Eng. 2020;8(47):17387-96.
- [25] Huang Z, Wang JJ, Chen Y, Wei N, Hou Y, Bai WD, et al. Effect of water-soluble dietary fiber resistant dextrin on flour and bread qualities. Food Chem. 2020;317:126452.
- [26] Mehboob S, Ali TM, Sheikh M, Hasnain A. Effects of cross linking and/or acetylation on sorghum starch and film characteristics. Int J Biol Macromol. 2020;155:786-94.
- [27] Verma A, Joshi K, Gaur A, Singh VK. Starch-jute fiber hybrid biocomposite modified with an epoxy resin coating: fabrication and experimental characterization. J Mech Behav Mater. 2018;27:5-6.
- [28] Wen XX, Shen MJ, Bai YJ, Xu CL, Han XL, Yang HL, et al. Biodegradable cell-laden starch foams for the rapid fabrication of 3D tissue constructs and the application in neural tissue engineering. J Biomed Mater Res B. 2020;108(1):104-16.
- [29] Yoshida S, Kondo K. Fiber volume control of composite materials by loss angle. Polym Compos. 2016;37(5):1307-11.
- [30] Gaudin R, Knipfer C, Henningsen A, Smeets R, Heiland M, Hadlock T. Approaches to peripheral nerve repair: generations of biomaterial conduits yielding to replacing autologous nerve

- grafts in craniomaxillofacial surgery. Biomed Res Int. 2016;2016:3856262.
- [31] Jiang CQ, Hu J, Xiang JP, Zhu JK, Liu XL, Luo P. Tissue-engineered rhesus monkey nerve grafts for the repair of long ulnar nerve defects: similar outcomes to autologous nerve grafts. Neural Regen Res. 2016;11(11):1845-50.
- [32] Malda J, Visser J, Melchels FP, Jungst T, Hennink WE, Dhert WJ, et al. 25th anniversary article: engineering hydrogels for biofabrication. Adv Mater. 2013;25(36):5011-28.
- [33] Annabi N, Nichol JW, Zhong X, Ji CD, Koshy S, Khademhosseini A, et al. Controlling the porosity and microarchitecture of hydrogels for tissue engineering. Tissue Eng Part B Rev. 2010;16(4):371-83.
- [34] Haque MA, Kurokawa T, Gong JP. Super tough double network hydrogels and their application as biomaterials. Polymer. 2012;53(9):1805-22.
- [35] Drury JL, Mooney DJ. Hydrogels for tissue engineering: scaffold design variables and applications. Biomaterials. 2003;24(24):4337-51.
- [36] Smith AM, Shelton RM, Perrie Y, Harris JJ. An initial evaluation of gellan gum as a material for tissue engineering applications. J Biomater Appl. 2007;22(3):241-54.
- Wu XF, Li W, Chen K, Zhang DK, Xu LM, Yang XH. A tough PVA/ HA/COL composite hydrogel with simple process and excellent mechanical properties. Mater Today Commun. 2019;21:100702.
- Fukushima K. Functionalization and precise synthesis of biodegradable polymers towards biomedical applications. Sen-I Gakkaishi. 2016;72(12):P571-3.
- [39] Ding HX, Cheng YZ, Niu XL, Hu YC. Application of electrospun nanofibers in bone, cartilage and osteochondral tissue engineering. J Biomat Sci Polym E. 2020;110:1-4.
- [40] Ismail NA, Amin KAM, Razali MH. Novel gellan gum incorporated TiO₂ nanotubes film for skin tissue engineering. Mater Lett. 2018;228:116-20.
- [41] George N, Geller HM. Extracellular matrix and traumatic brain injury. J Neurosci Res. 2018;96(4):573-88.
- [42] Malda J. Engineering of hydrogel-based bioinks for the fabrication of cell-laden 3D constructs. Hum Gene Ther. 2013;24(12):A27.
- [43] Lozano R, Stevens L, Thompson BC, Gilmore KJ, Gorkin R, Stewart EM, et al. 3D printing of layered brain-like structures using peptide modified gellan gum substrates. Biomaterials. 2015;67:264-73.
- [44] Park H, Guo X, Temenoff JS, Tabata Y, Caplan AI, Kasper FK, et al. effect of swelling ratio of injectable hydrogel composites on chondrogenic differentiation of encapsulated rabbit marrow mesenchymal stem cells in vitro. Biomacromolecules. 2009;10(3):541-6.
- [45] Akkineni AR, Ahlfeld T, Funk A, Waske A, Lode A, Gelinsky M. Highly concentrated alginate-gellan gum composites for 3d plotting of complex tissue engineering scaffolds. Polymers-Basel. 2016;8:5.
- [46] Shi WL, Sun MY, Hu XQ, Ren B, Cheng J, Li CX, et al. Structurally and functionally optimized silk-fibroin-gelatin scaffold using 3d printing to repair cartilage injury in vitro and in vivo. Adv Mater. 2017;29:29.
- [47] Peng YM, Liu QJ, He TL, Ye K, Yao X, Ding JD. Degradation rate affords a dynamic cue to regulate stem cells beyond varied matrix stiffness. Biomaterials. 2018;178:467-80.